Order of magnitude wall time improvement of variational methane inversions by physical parallelization: a demonstration using TM5-4DVAR

Sudhanshu Pandey[1,*], Sander Houweling[2], Arjo Segers[3]

[1]SRON Netherlands Institute for Space Research, Utrecht, the Netherlands
[2]Department of Earth Sciences, Vrije Universiteit Amsterdam, Amsterdam, the Netherlands
[3]TNO Department of Climate, Air and Sustainability, Utrecht, The Netherlands

*now at Jet Propulsion Laboratory, California Institute of Technology, Pasadena, CA, USA

Correspondence to: Sudhanshu Pandey (s.pandey@sron.nl)

Abstract. Atmospheric inversions are used to constrain the emissions of trace gases from using atmospheric mole fraction measurements. The four-dimensional variationalvariational (4DVAR) inversion approach allows optimization of the emissions at a much higher temporal and spatial resolution than the ensemble or analytical approaches but provides limited opportunities for scalable parallelization because it is an iterative optimization methodas the optimization is performed iteratively. Multidecadal variational inversions are needed used to optimally extract information from the long measurement records of long-lived atmospheric trace gases like carbon dioxide and methane. However, the wall clock time needed—up to months—complicates these multidecadal inversions. The physical parallelization (PP) method introduced by Chevallier (2013) addresses this problem for carbon dioxide CO_2 inversions by splitting the time period of the chemical transport model into blocks and running them that are run in parallel. Here we present a new implementation of the PP physical parallelization for variational inversion (PPVI) method approach that which is is suitable for methane inversions as it accounts for the chemical sink of methane's atmospheric lifetime. The performance of the PPVI method is tested in an 11-year inversion using a TM5-4DVAR inversion setup that assimilates surface observations to optimize methane emissions at grid-scale. Our PP implementation improves the wall time performance by a factor of 5We find that the PPVI inversion approach improves the wall clock time performance by a factor of 5 and shows excellent agreement with the posterior emissions of a full serial inversion with in an identical configuration (global mean emissions difference = 0.06 % with an interannual variation correlation R = 0.99 %; regional mean emission difference < 5 % and interannual variation R > 0.945). The wall clock time improvement of using the PPVI method method increases with the size of the inversion period. The PPVI approach method is planned to be used in future releases of the CAMS (Copernicus Atmosphere Monitoring Service (CAMS)) multidecadal methane reanalysis.

1 Introduction

Methane (CH_4) is the second- most important greenhouse gas after carbon dioxide (CO_2), and its atmospheric abundance has increased by more than a factor of 2.5250 % since preindustrial times. Due to its strong global warming potential, Methanit is responsible for 25 % of the anthropogenic radiative forcing in spite ofdespite its 200 times lower abundance than CO_2 due to its strong global warming potential (Myhre et al., 2013). Unlike the relatively steady increase in CO_2, mainly due to fossil fuel emissions, the methane observational record shows remarkable variability in growth rate. The causes of these variations are still debated (Rigby et al., 2017; Schaefer et al., 2016, Worden et al., 2017; Pandey et al., 2017).

Atmospheric inversions provide calculate

Reducing anthropogenic methane emissions has been recognized as an important requirement for achieving the 2015 Paris Agreement target of limiting global temperature rise to below 2° C relative to pre-industrial times (Ganesan et al., 2019; Nisbet et al., 2018). Climate change mitigation and adaptation strategies require reliable knowledge of the methane budget. The mmethane emission estimatess have been estimated using multidecadal inversions, which by optimally combininge the information in atmospheric observations and bottom-up emissions- emission estimates estimates (estimates using process-based models and inventories) along with corresponding error characteristics. Inversions useing a CTM (Cehemical transport models (CTM's)) simulate the spatiotemporal distribution of the methane concentrationsmole fractions in the atmosphere for a given set of emissions while also accounting for its atmospheric sink. Inversions use CTM's are used to disentanglcing the influences of atmospheric transport from the influences of, and sourcesemissions and sinks on the observed mole fractions (Naus et al., 2019, Pandey et al., 2019). Inversions have been performed on multidecadal scales to assess the information content of long records of methane mole fractions. For example, "The Global Methane Budget 2000–2017" (Saunois et al., 2020) presents regional emission estimates from nine different inversion setups. The methane emissions reanalysis project under the Copernicus Atmosphere Monitoring Service (CAMS) performs multidecadal inversions using the TM5-4DVAR variational approach to provide regularly updated gridded methane emissions (Segers and Houweling, 2020). Such multidecadal inversions have been performed, for example, for the "The Global Methane Budget 2000–2017" that was published recently by the Saunois et al. (2020). This study made methane emissions available from nine different inversion setups. The methane emissions reanalysis project under the Copernicus Atmosphere Monitoring Service (CAMS) performs multidecadal inversions using the TM5-4DVAR variational approach to provide regularly updated gridded methane emissions (Segers and Houweling, 2020).

Trace gas Emission

Atmospheric Iiinversions inversions that estimate CH_4 emissions adjust a state vector, which includes (consisting of gridded emissions or emission correction factors (and sometimes also the initial mole fraction field and other parameters in some inversions), to improve the agreement between model simulations and observations. These inversions use a CTM to simulate

the spatiotemporal distribution of the tracer in the atmosphere for a given set of emissions while also accounting for its atmospheric sink. They inversionsA minimize a Bayesian cost function that cost function is defined based on the difference between the modelled and observed mole fractions as well as the magnitude of the emission adjustments, weighted with respective error covariances. The solution of the inverse problem is posterior emission vector, which minimizes the cost function. There are three main minimization approaches used in atmospheric inverse modelling: analytical, ensemble and variational. The analytical approach is based on a closed-form solution of Bayes' theorem (Gurney et al., 2002). It requires the calculation of observation-sensitivities of each of the state vector elements separately. Thcis leads to a large computational cost involved and restrictss the approach'sits usage application to inversion problems with small sized state vectors. The ensemble approach improves the computational performance by representing parameterizing the state vector sensitivities usingby a statistical ensemble (Peters et al., 2005). Still only a relatively small sized state vector can currently be afforded using this approach.

The variational inversion approach was introduced to lift the state vector size restriction , using the adjoint of the CTM (Chevallier et al., 2005).

In the variational this approach, the minimum of a the cost function minimum is computed using an iterative procedure, with each iteration that comprisinges of a forward and an adjoint CTM run. The method has the advantage over the analytical approach in that it can be applied to non-linear inverse problems. Truncated posterior uncertainties can be obtained forfrom variational inversions using the conjugate gradient minimizer for linear inverse problems (Meirink et al., 2008). A more robust, but computationally expensive, estimate of posterior uncertainties can be obtained using a Monte Carlo method (Chevallier et al., 2007, Pandey et al., 2016). However, aAs each iteration of a variational inversion uses the output of the previous iteration,, there are limited opportunities for scalable parallelization in variational inversions, and these the calculations can take months depending on the spatial and temporal resolution of the inversion. Thise long wall clock time limits the resolution, the durationmaximum time range, andor the number of iterations that can be used in multidecadal variational inversions.

To improve reduce this longe wall timecomputational effieiency for of multidecadal variational CO_2 inversions carbon dioxide (CO_2) inversions, Chevallier (2013) introduced the physical parallelization (PP) method. In this method, which the timeseries full inversion period is of forward and adjoint CTM runs within each iteration aresplit divided into a number of blocks, and the CTM runs for the blocks and that are performed run in parallel within each iteration and. a. tmospheric mass eCorrectionsCorrections factors are added to the simulated CO_2 tracer mole fractions in a block applied after the CTM block runs are finished to account for changes in the background mole fractions due to net for emissions adjustments (iteration minus prior emissions) changes released in earlier blocks. This method reduceds the wall clock time by an order of magnitude (seven-

fold improvement for a 32-year inversion) while keeping the inversion-derived emission adjustments statistically consistent with a serial inversion. ~~However,~~ However, the original implementation of the PP~~their~~ method cannot be used for~~ a cannot be applied directly to~~ reactive trace gas like methane ~~methane~~ as the method~~it~~ does not account for atmospheric~~ chemical sink.

~~the limited chemical lifetime of methane of about 10 years, due to oxidation by the OH radicals in the atmosphere.~~ Here we ~~report~~ present an ~~extension~~ improved PP ~~of the~~ method that accounts for the limited atmospheric lifetime of reactive trace gases such as methane, which has an atmospheric lifetime of about 9 years (mainly due to oxidation by the OH radicals). ~~the atmospheric lifetime.~~ The intention is to use this new PP implementation for the Copernicus Atmosphere Monitoring Service (CAMS) methane flux reanalysis, which aims to provide ~~every year~~ annually ~~an~~ updated multi-decadal emission estimates ~~inversion,~~ within a production cycle ~~window~~ of only a few months. ~~The method is referred to as PPVI (physical parallelization for variational inversion) from here on.~~

In the next section, we present our ~~the~~ PP~~VI~~ method. ~~In Section 3, we~~The method's ~~test the~~ performance is tested ~~of the PPVI inversion method~~ using an 11-year ~~test~~ inversion~~s~~ setup presented in Section 3.~~.~~ The wall time and optimized emissions of a PP inversion are compared to a serial inversion in an identical configuration. ~~We compare the wall clock time and optimized emissions of a serial inversion with a PPVI inversion.~~In Section 4, we discuss possible future improvements and applications of the PP method. ~~We discuss the current CAMS methane inversion setup, and possible improvements and applications of the PPVI method in Section 4.~~ Our conclusions are summarized in Section 5.

2 Physical parallelization for methane inversions~~for variational inversions~~

An ~~In the 4D-var approach,~~inversion of an atmospheric trace gas ~~The~~ the solution of a~~atmospheric methane inverse problems of a trace gas is calculated by~~ minimize~~sing~~ ~~the~~ a Bayesian cost function of the state vector $\boldsymbol{x}$:

$$J(\boldsymbol{x}) = \frac{1}{2}\,[\boldsymbol{x}-\boldsymbol{x}^a]\mathbf{B}^{-1}[\boldsymbol{x}-\boldsymbol{x}^a] + \frac{1}{2}[\boldsymbol{m}\boldsymbol{H}(\boldsymbol{x}) - \boldsymbol{y}]\,\mathbf{R}^{-1}[\boldsymbol{H}(\boldsymbol{x})\boldsymbol{m} - \boldsymbol{y}] \quad \text{.....(1)}$$

Here ~~In here,~~ $\boldsymbol{y}$ is the observation vector, and~~,~~ $\boldsymbol{x}^a$ is the prior~~i~~ state vector. $\mathbf{B}$ and $\mathbf{R}$ are the error covariance matrices of the prior emissions and the observations, respectively. ~~For methane emission inversions,~~The vector $\boldsymbol{m}$ constitutes the modelled mole fractions corresponding to $\boldsymbol{y}$~~The the observation operator H consists of the a CTM run that simulates methane mole fractions at time and location of $\boldsymbol{y}$. given~~

~~and **R** are the error covariance matrices of the~~ prior state~~a priori emissions and the observations, respectively.~~ . It is computed using a CTM operator H, which simulates the mole fractions given the emissions in the state $\boldsymbol{x}$ and the initial mole fraction field $\boldsymbol{c}_0$.

$$\boldsymbol{m} = H(\boldsymbol{c}_0, \boldsymbol{x}) \quad \text{.....(2).}$$

In a variational inversion setup, the posterior solution ~~x^p~~ of Equation~~.~~ (1) is ~~found~~ obtained by minimizing J using an iterative procedure that computes a ~~estimates~~new emission update ~~a new~~ $\boldsymbol{x}^{i+1}$ in ~~in~~ each iteration i using the gradient ~~of J:~~

$$\nabla J(\boldsymbol{x}^i) = \mathbf{B}^{-1}[\boldsymbol{x}^i - \boldsymbol{x}^a] + H^{*T}(\mathbf{R}^{-1}[\boldsymbol{m}^i - \boldsymbol{y}]) \quad \text{.....(32).}$$

~~where,~~ H^{*T} represents the adjoint CTM operator, which is implemented using the adjoint code of the CTM. The inversion finishes when a predefined convergence criterion is met, such as a desired gradient norm reduction or simply a maximum number of iterations.

~~In a serial variational inversion the observation operator iteration i, the CTM H simulates a mole fraction vector $\boldsymbol{m}^i$ with mole fractions representing the observations for observation vector $\boldsymbol{y}$, based on using the initial mole fraction field $\boldsymbol{c}_0$ and emission estimates $\boldsymbol{x}^i$ of iteration i:~~

~~$$\boldsymbol{m}^i = H(\boldsymbol{c}_0, \boldsymbol{x}^i) \quad \text{.....(3)}$$~~ ~~[SP1]~~

In the PP~~VI~~ method presented in Chevallier (2013), ~~,~~ the full ~~period~~ period of the ~~CTM~~ inversion is split ~~is broken~~ into r overlapping time ~~blocks~~blocks, which can be ~~are~~ run in parallel. Figure 1 ~~shows a~~ schematically represents ~~diagram of~~ the main steps in ~~of~~ the PP~~VI~~ method used in the forward mode to calculate $\boldsymbol{m}^i$. At the start of the inversion, a serial CTM run ~~is performed serially~~ (without ~~blocks~~segmentation) is performed ~~first~~ ~~in order~~ to calculate initial mole fraction fields $\boldsymbol{c}_k^a$ for each block k using the ~~a~~ prior~~i~~ emissions $\boldsymbol{x}^a$~~. This CTM run can be performed at coarser resolution than the main inversion to save time.~~. In an iteration, mole fractions for the iteration~~CTMA mole fraction vector~~ $\boldsymbol{m}_k^i$ is ~~then~~ computed using the block observation operator H_k, ~~computes the mole fraction vector $\boldsymbol{m}_k^i$ with~~based on the ~~latest~~ emission estimate from the previous iterations ~~$\boldsymbol{x}_k^i$, and~~ the initial mole fraction for this block,

~~The overlaps between consecutive blocks is kept, where modelled modeeled mole fraction from are needed for methane perturbations to uniformly distribute over the spatial domain of the CTM, such that each perturbation could be diagnosed by at least some observation sites. The mole fraction vector $\boldsymbol{m}_k^i$ for the observations $\boldsymbol{y}_k$ could now be calculated by using the~~

~~small CTM block H_k with emissions $\boldsymbol{x}_k^i$~~ and a mole fraction ~~a~~ correction ~~factor vector~~ n_k^i~~. which accounts for the state vector innovation in the preceding block.~~

:

$$\boldsymbol{m}_k^i = H_k\left(\boldsymbol{c}_k^a, \boldsymbol{x}_k^i\right) + n_k^i \quad \text{.....(4).}$$

Here the scalar~~The correction~~ n_k^i accounts for the ~~impact of~~ emission differences between the prior and the iteration in the ~~time~~ period ~~from~~ preceding the ~~to prece~~block~~ on the simulated observations within the block~~. The error due to this simplification is further reduced by using an overlap period between consecutive blocks, where modelled mole fractions from the succeeding block are discarded. The overlap period CTM run distributes the emission differences uniformly through the Earth's atmosphere. The PP method by Chevallier (2013) was applied to CO_2 inversions, where n_k^i was simply calculated as the sum of the emission differences from each preceding block:

$$n_k^i = \sum_{l=1}^{k-1} f\,[|\boldsymbol{x}_l^i - \boldsymbol{x}_l^a|] \quad \text{...} \quad (5).$$

Here $|\boldsymbol{x}|$ denotes the global sum over elements of $\boldsymbol{x}$. f is a scalar used to convert emissions to mole fractions~~. f is calculated for a tracer by,~~ assuming a uniform distribution of the emitted trace gas throughout the Earth's atmosphere. f is calculated simply as the ratio between the number of moles in a unit emission and the number of moles of air in the atmosphere.

Methane has an atmospheric lifetime of about 9 years. Unlike CO_2, a large fraction of methane emission differences will be chemically removed within the duration of a multidecadal inversion as well as within a PP inversion block. Therefore, in our new implementation of the PP, we use a mole fraction correction vector~~The correction~~ $\boldsymbol{n}_k^i$ (with size of $\boldsymbol{m}_k^i$) instead of the scaler n_k^i to apply separate corrections to each observation. We account for the ~~also~~ limited lifetime of methane by implementing an atmospheric sink operator S. In addition, we use ~~we implement~~ a CTM block sensitivity vector $\boldsymbol{h}_k$~~, is implemented,~~ distribute global emission changes more precisely, ~~as per~~ taking into account the full 3D atmospheric transport and the sink rather than assuming a globally uniform distribution. $\boldsymbol{h}_k$ is computed at the start of the inversion by running H_k ~~(~~ in forward mode with a unit initial mole fraction field and zero emissions, i.e., $\boldsymbol{h}_k = H_k\,(\boldsymbol{c}_k = 1, \boldsymbol{x}_k = 0)$. ~~is calculated using an emission to mole fraction conversion factor $f = 0.361$ ppb/Tg and a methane sink operator S :~~

$\boldsymbol{n}_k^i$ is computed as

$$\boldsymbol{n}_k^i = \boldsymbol{h}\sout{\boldsymbol{H}}_k \sum_{l=1}^{k-1} S_{l,k}\,(f\,[|\boldsymbol{x}_l^i - \boldsymbol{x}_l^a|]) \quad \text{.....(6~~5~~).}$$

~~The scalarIn here, $\mathbf{H}_k$ is the CTM block sensitivity to a uniform initial mole fraction field perturbation, which is calculated at the start of the inversion by running each block with an initial unit mole fraction field and a zero emissions field.~~ $S_{l,k}$ accounts for the impact of atmospheric sinks on the global uniform concentration change at the start of block k, induced by emission ~~perturbations~~ differences ~~during the~~within block l ~~till the start of the block k.~~. ~~Thereafter~~Within block k itself~~on~~, the impact of atmospheric sinks~~, as well as atmospheric transport,~~ is accounted for by ~~$\boldsymbol{h}_k \mathbf{H}_k$. We parameterize $\boldsymbol{S}_{l,k}$ with an e-folding decay function with atmospheric lifetime of methane of 9 years, which was found to be sufficient for our test inversion (Section 3).~~

~~In~~ ~~E~~each iteration of a variational inversion computes a departures vector $\delta\boldsymbol{m}$:

$$\delta\boldsymbol{m} = \mathbf{R}^{-1}[\boldsymbol{m} - \boldsymbol{y}]$$ ~~, the modelled mole fractions from the forward CTM run are used to calculate departures, i.e., the~~ ..... (7).

~~difference between observations and the modelled mole fractions scaled with the respective errors. Thereafter,~~ ~~T~~the adjoint CTM H^* is run with $\delta\boldsymbol{m}$ ~~uses these departures~~ to compute ~~calculate~~ the local gradient of the cost function (Equation~~uation~~ 2). In the PP~~VI~~ method, H^*~~, the adjoint CTM~~ is split into blocks ~~of~~covering the same periods ~~blocks are kept the same~~ as~~as~~ used for the forward CTM simulation ~~blocks and Equation 2 is applied in adjoint mode~~. In an iteration, ~~First,~~ each adjoint block is first run with the respective departures. Then, the modelled adjoint sensitivities of a block $\delta\boldsymbol{x}^i_{k,l}$ ~~of block k~~ are adjusted for the effects of departures of succeeding ~~successive~~ blocks by adding adjoint mole fraction correction scalar~~s~~ $g^i_k \delta\boldsymbol{n}^i_t$ ~~calculated using as follows~~:

~~$g\delta\boldsymbol{n}^i_k = f \sum_{l=k+1}^{r} S^*_{k,l} (-\boldsymbol{h}\mathbf{H}^{T*}_l (\delta\boldsymbol{m}^i_l))$~~ ..... ~~(86)~~.

The correct adjoint implementation of the ~~adjoint part of the~~ PP~~VI~~ method ~~was~~ can be verified using the adjoint test (Meirink et al., 2008). The test checks for the equality~~.~~

$$\langle M(\boldsymbol{a}), \boldsymbol{b} \rangle = \langle \boldsymbol{a}, M^*(\boldsymbol{b}) \rangle$$ ..... (9),

where M and M^* denote the forward and adjoint model operators, $\langle\ \rangle$ denotes the inner product. $\boldsymbol{a}$ and $\boldsymbol{b}$ are the arbitrary forward and adjoint model states.

In a PP~~VI~~ inversion, the initial mole fraction field $\boldsymbol{c}_0$ needs to be consistent with the observations as a discrepancy between the two leads to large emission ~~adjustments~~ differences in the early months of the inversion period. This issue can easily be dealt with in a serial inversion using a spin-up period and rejecting this period from the posterior solution. However, in a PP~~VI~~ inversion, the large emission differences ~~adjustments~~ may result in large mole fraction correction~~s factors~~, which increases the error in the PP~~VI~~ approximation (see Equations~~uation~~ 4 & 5). This can be avoided by taking a realistic $\boldsymbol{c}_0$ from ~~another~~another inversion covering the period before the PP~~VI~~ inversion.

In summary, the main steps of ~~a~~ the PP~~VI~~ methane inversion are as follows:

1. Construct an initial mole fraction field $\boldsymbol{c}_0$ consistent with observations at the start of the inversion.
2. ~~Divide~~ Split the full period of the inversion into *r* over-lapping time blocks.
3. To calculate ~~Calculate the initial mole fraction fields ($\boldsymbol{c}_k^{a\theta}$,) for each block by Calculate the initial mole fraction fields ($\boldsymbol{c}_k^{\theta}$) for each block by r~~running the forward CTM serially with ~~the~~ prior ~~a priori~~ emissions $\boldsymbol{x}^a$ and sav~~e~~ing the simulated mole fraction fields at the start time of each block.
4. Calculate the CTM block sensitivities ~~($\boldsymbol{hH}_k$)~~ by running the CTM over each block~~s~~ with a ~~unity~~ uniform initial mole fraction field of 1 and zero emissions, and sample~~ing~~ the model output at the observation time and location~~s~~.
5. Perform the inversion by iteratively minimizing the cost function until the convergence ~~criteria~~condition is met using a forward and an adjoint run in each iteration:
   a. Forward run:
      i. Run all ~~the~~ forward CTM ~~for each~~ block~~s~~ in parallel with the initial mole fraction fields from ~~the~~ step 3.
      ii. Account for the emission ~~differences~~ changes relative to ~~from~~ the ~~a~~ prior~~i~~ in preceding blocks~~,~~ by ~~applying~~ adding the ~~mole fraction~~ corrections $\boldsymbol{n}_k^i$ (Equation 54).
   b. Adjoint run:
      i. Run ~~the~~ all adjoint CTM ~~for each~~ block~~s~~ in parallel to calculate the adjoint emission~~s~~ sensitivitie~~s.s~~ ~~$\delta \boldsymbol{x}_t^i$.~~
      ii. Add~~Apply~~ the adjoint correction~~s~~ $g_k^i \delta \boldsymbol{n}_t^i$ to account for the effect of departures in successive blocks (Equation 8~~6~~).

The CTM run~~s~~ in the steps 4, 5.a.i and 5.b.i are performed in parallel. The steps without CTM run (1, 2, 5.a.ii and 5.b.ii) require very little wall time. Step 3 is the most time-consuming because a full serial CTM run is performed in the step. To reduce the wall time, this run can be performed at a coarse CTM resolution. This will not have a major impact on the inversion's performance as the coarse resolution mole fraction fields would be consistent with the source, sink and large-scale atmospheric

transport patterns, and $\boldsymbol{m}$ is sampled after the coarse field is transported by a high-resolution CTM block runs during the overlap periods.

3 PP ~~VI~~ p~~P~~erformance test

~~In this section,~~ W~~w~~e evaluate the ~~the~~ performance of the PP~~VI~~ method by comparing a PP inversion with ~~against~~ a serial methane inversion. Both inversions are performed for an 11-year period (1999-2010) with identical observations and prior emissions. We ~~We perform the inversions for a 11 year period (1999-2010)~~ us~~ing~~ the TM5-4DVAR inversion system (Bergamaschi et al., 2010; Meirink et al., 2008, Krol et al., 2005) ~~, which consists of the TM5 (Transport Model version 5; Krol et al., 2005)~~ with the settings used in Pandey et al. (2016). The TM5 CTM is run at 6° × 4° horizontal resolution and 25 vertical hybrid sigma-pressure levels from the surface to the top of the atmosphere. The meteorological fields for this offline model are taken from the European Centre for Medium-Range Weather Forecasts (ECMWF) ERA-Interim reanalysis (Dee et al., 2011). We optimize a single category ('total') of methane emissions at 6° × 4° spatial resolution and monthly temporal resolution. The posterior emissions of the two inversions are compared after integrating over the TRANSCOM regions shown in Figure 2a.

The inversion assimilates surface observations from the NOAA Earth System Research Laboratory (ESRL) global cooperative air sampling network at on- and off-shore sites (Dlugokencky et al., 2011; Dlugokencky et al., 2020). The locations of the observation sites~~s~~ are shown in Figure 2b. The prior covariance matrix $\mathbf{B}$ is constructed assuming relative emission uncertainties of 50 % per grid box per month. The emissions are assumed to be correlated temporally using an exponential correlation function with an e-folding time scale of 3 months, and spatially with a Gaussian correlation function using a length scale of 500 km (Houweling et al., 2014). Uncertainties of 1.4 ppb are assigned to ~~the~~ ~~CH_4~~methane observations. Our system also assigns a model~~l~~ing representation error based on simulated local mole fractions gradients (Basu et al., 2013). The prior emissions are taken from the same sources as in ~~, same as in~~ Pandey et al. (2016). ~~,~~ The emissions ~~of~~ in 2008 ~~are~~ applied to every year in the inversion ~~time~~ period, h~~, h~~ence there is no interannual variability in the prior emissions. ~~-~~ The cost function J is minimized using the conjugate gradient minimizer, which is based on the Lanczos algorithm (Fisher and Courtier, 1995). The inversions use the convergence criterion of gradient norm reduction by a factor 1000, which is achieved after 19 iterations in both inversions.

In the PP~~VI~~ inversion, we ~~divide~~ split the inversion period of 1999-2010~~,~~ into 11 blocks of ~~of~~ 21 ~~-~~month~~ss with 9 months overlap between successive blocks~~. ~~Effectively,~~ The first 9 months of each block is the overlap period used for uniformly mixing the emission changes within the atmosphere, while the last 12 months ~~each block~~ provide~~s~~ modelled mole fractions for assimilating the observations~~for one year~~.~~.~~ We parameterize the sink operator S (Equation 6) with an e-folding decay function

with a constant 9-year atmospheric lifetime of methane. sufficient for our test inversion (Section 3). The input emissions of TM5 are mass fluxes (Tg yr^{-1}) and the output is in mole fractions (ppb). The methane emission changes are converted in mole fractions using an $f = 0.361$ ppb/Tg. The Ssuccessful implementations of the PPVI method in the adjoint mode on this TM5-4DVAR setup was verified using the adjoint and gradient test (Equation 9)s. The next section (3.1) compares evaluates the observation-model mismatches and posterior emissions differences between the PP and serialtwo inversions, and the section thereafter (3.2) presents the wall clock time improvement by achieved of usingby the PP VI methodinversion.

3.1 Emission estimation errors

Here we compare examine the quality of the inversion-optimized fit to the observation.the observation fit and the posterior emissions of the PPVI and serial inversions . Figure 3 shows the time series of the prior and posterior simulations and the observations for two background sites, representing one for each hemisphere: Barrow (Alaska) and the South Pole. The prior observation prior model RMSDE (root mean square errordifference) for Barrow (78 ppb) is 3 times higher than for the South Pole (28 pbb). The Barrow observations shows a more larger high-frequency variations than the the South Pole as the Northern Hemisphere station is influenced by methane emissions from wetlands. closer to methane sources. The PPThe simulatedVI mole fractions simulated by from the PP inversion results are are in good agreement with the results obtained from the serial inversion: an the RMSDsE of between the two is 2 ppb and 1 pbbis obtained for Barrow, and the of 1 pbb respectively for Barrow and South pole, respectively, which are only 2.5-% and 3.2-% of the prior initial observation prior RMSDmismatch. This shows that the PP inversion, starting from an identical prior, starting from an identical prior, the PPVI inversion is able to match the observations at these sites about as good as the serial inversion.configuration.

Figure 4 shows the average mole fraction differences at all observation sites. Figure 4 shows the probability density functions of the observation-model mismatch weighted with the uncertainties used in the inversion. The prior observation-prior prior RMSD for all observations combined mismatch is 67 ppb. The mean 6.7 ± 6, with negative mean mismatch is –58 ppb because the 2008 bottom-up emissions used as the prior are larger than the mean posterior emission over 1999-2010. The In the posterior solution of the serial inversion, the mismatch is reduced to −0.06 ± 1.24. average data- uncertainty (mean of the square root of the diagonal elements of **R**) is 19 ppb (not shown). For both inversions, a good model fit to the observations is achieved with a gradient norm reduction of 1000. The posterior simulation of both the serial and PP inversions reduce the RMSD to 20 ppb (mean = –2 ppb). PPVI mismatch The posterior (−0.06 ± 1.26) simulation is also very small and similar to the serial inversion. TThe minus mismatch RMSD between the PPVI and serial inversions is 1.9 ppb (mean = –0.1(0.005 ppb ±), which is0.23) an is an order of magnitude smaller than the observationposterior minus prior RMSD of 62 ppb (mean = –55 ppb) mismatch. This, which shows that the implementation of the PPVI method has does not have a significantlittle impact

~~impact~~ on the inversion ~~system~~'s ability to fit the observations. ~~For both inversions, the good fit to the observations also confirms that a gradient norm reduction of 1000 is sufficient.~~

A good agreement between observations and posterior models do~~es~~ not guarantee ~~necessary mean~~ that the inversions have produced similar posterior emissions. The physically parallelized CTM used ~~transport model~~ in~~of~~ the PP~~VI~~ inversion has lost some of the consistency of the full ~~is a simplification of the "perfect" transport model~~CTM ~~of~~ used in the serial inversion. If the impact of this simplification is small, the posterior emissions of the two inversions should be in good agreement. Figure 5 shows ~~the~~ mean emission~~s estimates~~ (averaged over 1999-2010) from~~of~~ the inversions integrated over the globe and over ~~the~~ TRANSCOM regions. The serial inversion adjusts the global mean prior emissions of 544 ± 11 Tg yr^{-1} by –22 Tg yr^{-1}. The ~~The mean global emissions of the~~ PP~~VI~~ inversion is~~and serial inversions are in~~ in excellent agreement with the serial inversion in ~~with~~ this respect. The two differ by ~~with <~~ 0.3 Tg yr^{-1} (0.0~~65~~ %) ~~difference~~, which is~~.~~ 1-% of the difference between prior and posterior emissions from the serial inversion. The global methane emissions are in general~~ly~~ well constrained by the NOAA observations in a ~~the~~ serial inversion, and ~~PPVI inversions meaning~~ ~~that~~ the additional error introduced by ~~in~~ the PP method~~VI approach~~ does not seem to have a significant impact ~~the constraint~~ on the ~~emissions at the~~ global emissions ~~scale~~. At regional scales~~-~~, the serial inversion adjustment is the smallest for Australia: + 0.4 Tg yr^{-1} for a prior of 6.6 ± 0.4 Tg yr^{-1}. The PP inversion adjusts the prior here by 0.5 Tg yr^{-1}, implying that the difference with the serial inversion (0.1 Tg yr^{-1}) is well within the prior emission uncertainty. The serial inversion changes the Eurasian temperate emissions the most, by –58 Tg yr^{-1}, where prior emissions are 135 ± 8 Tg yr^{-1}. The PP inversion changes these emissions by –60 Tg yr^{-1}, i. e., a difference of 2 Tg yr^{-1} and well within the prior uncertainty also. The South American temperate region has the largest difference between the serial and PP emission estimates of 2 Tg yr^{-1}. The serial emissions for this region are 6.5 Tg yr^{-1} higher than the prior of 36 ± 2.4 Tg yr^{-1}. In summary, ~~The~~mean ~~performance of PPVI in other TRANSCOM regions is also good for mean~~ PP emission~~s~~ estimates for the TRANSCOM regions deviate within < 5 % ~~deviation~~ from the serial emissions ~~inversion~~.

~~On average, the deviations are within 30% of the posterior uncertainty.~~ Figure 6 shows the inter-annual variability of the emission estimates. ~~Due to the large observational constraint,~~ T~~t~~he global emissions time series of the PP and serial ~~two~~ inversions show a very good ~~the best~~ agreement with a correlation coefficient R = 0.99, explained by the large observational constraint. Over the TRANSCOM regions, the North American temperate region has the best agreement (R = 1.0). All other regions have ~~an~~ R ~~better~~higher than 0.98 except for Australia (0.96) and Europe (0.94). Figure 7 shows the intra-annual variations of the emissions. At the global scale, the PP and serial time series match very well with R = 1.00, whereas R between prior and serial is 0.93. The agreement between PP and serial time series is also very good for all TRANSCOM regions (R > 0.98) despite low correlations between prior and serial emissions for some regions, for example, R = 0.13 for the South American temperate region. This shows that the PP inversion is able to reproduce the seasonal cycle of the emissions very well. In summary, the combination of small differences in the mean emissions, and the high correlations between intra- and

inter-annual time series, shows that the PP inversion can effectively reproduce results of the serial inversion. ~~the agreements are also good with $R > 0.95$.~~

3.2 ~~Computational cost~~Wall time

Table 1 compares the wall ~~clock~~ times used ~~needed~~ by ~~for~~ the ~~PPVI~~PP and serial inversions. ~~Our~~ The TM5 model in our inversion setup ~~runs~~ uses OpenMP parallelization and ~~gives~~gave the best wall time ~~clock~~ performance on 4 CPUs on a single node. Using more CPUs reduces the performance as the communication overhead within the CPUs becomes the bottleneck. ~~.~~ (Note that the TM5-MP version ~~described~~ in Williams et al., 2017, with improved parallel scaling, was not used in this study). In this configuration, a forward or adjoint TM5 CTM run of one year took ~~takes~~ about 15 minutes. Hence an iteration of the serial inversion, consisting of 11 years forward and adjoint runs, require~~ds~~ 5 hours. The ~~PPVI~~PP inversion iterations ~~are~~ were performed in 11 parallel blocks of 21 months each on 4 CPUs. A single ~~PPVI~~PP iteration took ~~takes~~ 55 mins, which is > 5 times faster than the serial inversion. ~~Both inversions achieved a gradient norm reduction of 1000 in 19 iterations. The PPVI inversion runtime is given in Table 1, including the time needed for (1) a serial TM5 forward run for the initial mole fraction fields (2) a block run for the initial mole fraction sensitivities.~~ The main steps of PP implementation are listed in Section 2. In our inversion test, the initial mole fraction fields c_0 (step 1) were taken from an inversion using surface measurements that was not performed in this study. Steps 1, 2, 5.a.ii and 6.a.ii took negligible time. Step 3 took 2.5 hours because it consists of a full serial TM5 forward run. Steps 4, 5.a.i and 6.a.i consist~~ing~~ of 11 ~~21 month~~ TM5 ~~simulations~~run over blocks ~~over~~of ~~-~~21 months which were run in parallel and~~,~~ took ~~this~~ 25 minutes each. Note that an iteration took longer than the sum of the forward and adjoint block runs because of a few minutes waiting time for the computer cores to become available again. ~~Overall,~~ In total, the ~~PPVI~~PP inversion took~~takes~~ 20 hours, ~~or~~ 5 times less than the serial inversion which took ~~(~~101 hours~~)~~. Note that although the PP inversion took a shorter wall time, it needed extra CPU core hours for the additional 9-month overlap, CTM block sensitivity and initial mole fraction computation runs. The PP inversion used a total of 700 CPU core hours, whereas the serial inversion used about 400 CPU core hours. Table 1 also provides a ~~n estimate~~projection of the wall ~~clock~~ time improvement of a hypothetical 35-year inversion~~s~~ (not performed in this study) based on the ~~using the~~ TM5-4DVAR inversion setup used in this study. ~~For such a long period, A~~a ~~PPVI~~PP inversion would be 15 times faster for such a long period.

Overall, we find that the ~~PPVI~~PP method, which account~~s~~ for the atmospheric lifetime of methane, is able to effectively reproduce the posterior emissions of a traditional 11 ~~-~~year~~s~~ serial inversion ~~well within its uncertainties in~~ 5 times ~~-~~faster~~less wall clock time~~.

4 Discussion

The utility of the PP method for inversion of a trace gas ~~emissions~~depends on the time scale of the influence of emissions on observations within the spatial domain of the CTM. Therefore, PP is mainly useful in global inversions of trace gases that have atmospheric lifetime of a year or longer in the atmosphere. For a trace gas with a shorter lifetime, such as of carbon monoxide with 2 months lifetime, emission perturbations last for a short duration. A multidecadal inversion of such a trace gas can be broken into many short inversions. These short inversions can be performed in parallel, and the posterior emission can be combined thereafter. A similar approach can be used for regional inversions of short-and long-lived trace gases because emission perturbations are quickly advected out of the regional CTM domain and hence do not influence observations for a long period.

4.1 Current CAMS inversion setup

In the future, the ~~PPVI~~PP method will be implemented in the CAMS ~~-~~multidecadal methane emissions reanalysis setup. The European Commission has anticipated the need for reliable information about atmospheric composition of greenhouse gases through development of numerical systems that combine sophisticated physical models with measurements from a wide range of observing systems for an operational service, which is being implemented. The current CAMS methane flux reanalysis product (Segers and Houweling, 2020) uses the TM5-4DVAR inverse modelling system and provides measurement-informed monthly methane emission estimates. The ~~product~~ latest release has two sets of methane emissions: (1) release v19r1 for 1990-2019 using surface observation; (2) release v19r1s for 2010-2019 using surface and also GOSAT satellite observations. The surface observations are mainly from the NOAA network (Dlugokencky et al., 2011). Methane emissions are optimized at 3° × 2° spatial resolution and monthly temporal resolution using TM5 with 34 vertical layers. If performed in serial mode each iteration of the 1990-2019 inversion would take about 5-10 days, and the full inversion will require multiple months to finish. Segers and Houweling (2020) circumvent this issue by breaking the full inversion into smaller inversions of 3-year time windows that are performed in parallel. The target inversion on high resolution (3° × 2° degrees, 34 layers) is preceded by a coarse resolution inversion (6° × 4°, 25 layers) that provides the initial mole fraction fields and is processed serially. The high-resolution inversion optimizes only the emissions and uses initial mole fractions for each 3-year block obtained from mole fraction fields of a coarse resolution inversion, which optimizes both emission and initial mole fractions. The 1990-2019 inversion using this approach still takes 3-4 months to finish~~,~~ and requires about 40 smaller inversions to provide the end result. These numbers depend of course on the parallel efficiency of the model and the computing server, but even if these are improved, the need for a serial sequence of inversions to provide a time~~s~~ series of initial mole fractions imposes a limitation to the model resolution that can be used. With the implementation of the ~~PPVI~~PP method presented in this study, the ~~computational~~ wall time performance of the CAMS reanalysis inversions will improve in~~if~~ future.

4.2 Possible further improvements

The ~~In the PPVI~~PP method~~, the wall-clock time of a CTM run in an inversion iteration is reduced by physical parallelization of the CTM into blocks. To~~ accounts for changes in the background mole fractions due to emission changes in ~~pervious~~preceding blocks using~~,~~ ~~the~~ a sink operator S, a ~~S,~~ a CTM block ~~-~~sensitivity ~~*h*y **BH B,**~~ and ~~the~~ an ~~-~~overlap~~s~~ between the consecutive blocks ~~are is used~~. In our test experiment, S is assumed to be an e-folding decay function with an atmospheric lifetime of methane of 9 years, which we ~~find is~~found to be sufficient for the annually-repeating OH field used in our 11-year CTM runs. ~~This might not be the case for multi-decadal inversions, in which th~~Me ~~m~~ethane lifetime within the duration of a longer multidecadal inversion will vary due to climatological influences~~,~~ as well as possible trends and interannual variations in the hydroxyl radical abundance. In such cases, S can be defined as a function of an annual lifetime vector for the specific CTM run. The lifetime vector can be calculated as the ratio of the annual sink and ~~mean~~ global methane burden simulated by~~in~~ the~~a~~ serial CTM run in step 3 of the PP method.

The overlap period between ~~the~~ consecutive blocks in the ~~PPVI~~PP method allows ~~a uniform mole fraction~~methane emission perturbations to mix within the CTM domain according to ~~the~~ atmospheric transport. We used a 9-month overlap in our test inversion ~~experiment~~ setup. It was ~~and found it to be~~ sufficient for optimizing emissions from large TRANSCOM regions ~~at annual scale (Figure 5 & 6) that are optimized~~ using the surface observations. The 6-month overlap ~~as~~ used by Chevalier et al. (2013) for CO_2 inversions was found to be insufficient for a PP methane inversion, likely because of the differences between the source and sink distributions of methane and CO_2. Increasing the overlap period to 9-month and using CTM block sensitivity vector solved this issue. We expect that a 1-year overlap, equal to the interhemispheric mixing time, would be more than sufficient for all tracers irrespective of their source-sink distribution and lifetime. A shorter overlap ~~, which~~ would improve ~~improves~~ the computational efficiencnt~~t~~ly and wall time but reduce~~s~~ the accuracy of the physical ~~CTM~~ parallelization of the CTM~~, could be used depending on the scales that are addressed by the inversion~~. The PP accuracy ~~can~~could be maintained with shorter overlap periods by using a mole fraction correction vector per hemisphere rather than the single global vector used in this study. ~~Although~~However, the computational resources and wall ~~clock~~ time saved by this would be~~this are are~~ partially ~~offset~~spent on ~~by~~ the additional block sensitivity~~ies~~ runs. Our ~~performance~~ test inversions are performed at a relatively coarse ~~resolution~~horizontal resolution of ~~of~~ 6° × 4° ~~horizontal resolution and~~with 25 vertical hybrid sigma-pressure levels. We do not expect the performance of the PP method to degrade significantly for higher resolution inversions if there is sufficient overlap between the blocks and the mole fraction~~mass~~~~mixing ratio~~ corrections are parameterized correctly. Furthermore, the performance gained by performing the inversions at higher resolution because of the improved computational performance will likely outweigh the accuracy loss due to the assumptions made in the PP method.

The PP method reduced the wall time of the CTM simulations in a variational inversion but introduces additional model errors because of the ~~simplifying~~simplifications made~~ assumptions made for simulation over long time periods to simulate long durations~~. For our test inversion setup, these PP-CTM model errors are minor as the posterior PP emission estimates are in good agreement with the serial estimates. In future PP implementations, these PP-CTM errors can be accounted for in the observation error matrix **R**. The PP-CTM error can be calculated as the difference between the model output of a PP and a serial forward CTM run with randomly perturbed prior emissions.

4.3 Methane sink optimization

The hydroxyl radical OH is the main sink of methane in the atmosphere. Zhang et al. (2018) showed that the satellite-observed atmospheric signature of the methane sink ~~from oxidation by OH~~ is sufficiently distinct from that of methane emissions, hence OH mole fractions can be optimized using synthetic shortwave infrared (SWIR) and thermal infrared (TIR) satellite observations. Following up on this, Maasakkers et al. (2019) and Zhang et al. (2021) used methane observations from the GOSAT satellite to optimize atmospheric OH fields along with methane emissions. These studies assume a quasi-linearity for the inversion ~~as~~as ~~the~~ changes to the methane mole fractions are expected to remain small compared to the mean.~~and OH are small in an inversion.~~ Under a quasi-linear ~~such conditions~~assumption,~~ OH can be optimized in a the PPVI~~PP methane inversion ~~method~~ by ~~can also be implemented in inversions optimizing OH. In such a PPVI implementation,~~ introducing annual OH scaling factors in the state vector and the ~~the~~ methane lifetimes in the sink ~~*S*~~ operator can ~~would~~ be scaled in each iteration to reflect the corresponding OH adjustments~~ to the. OH mole fractions.~~ Such an implementation can also be used in inversions optimizing OH using methyl chloroform ~~(CH_3CCl_3) and a CTM~~(~~, as for example performed by,~~ Naus et al., ~~(~~2021).

5 Conclusions

Regular surface observations of methane mole fractions started in ~~the~~ early 1984, and by now the measurement record spans more than 35 years (Dlugokencky et al., 2011). An atmospheric inversion with a very large state vector is needed to properly utilize the information in such long measurement records. The variational inversion approach allows for optimization of a much larger state vector~~s of a larger size~~ than the ensemble or analytical approaches. However, each iteration ~~step~~ of a variational inversion uses the ~~CTM~~ output of the previous iteration, limiting the opportunity for scalable parallelization. At the same time, an increase in the spatio-temporal resolution of CTMs~~, which is~~ needed to take full advantage of the rapidly improving precision and coverage of surface and satellite measurements~~,~~ results in a~~n exponential~~ rapid increase in wall ~~clock~~ time.

We have developed the ~~PPVI~~PP method for methane inversions which improves the wall ~~clock~~ time of variational methane inversions by ~~the application of~~ physical CTM parallelization while accounting for the atmospheric lifetime in forward and adjoint variational modes. We have tested the performance of this method using an 11-year TM5-4DVAR inversion ~~e modeling~~ setup that consists of a traditional serial inversion and a ~~PPVI~~PP inversion in~~of~~ an identical configuration ~~performed for a period of 11 years~~. The ~~PPVI~~PP method reduced the wall ~~clock~~ time by a factor of 5 ~~times and~~while still ~~showed~~showing excellent agreement with the posterior emissions ~~of the~~from the~~an equivalent~~ serial inversion. The wall ~~clock~~ time improvement of using ~~PPVI~~PP will be even larger for longer inversions, for example, by a factor of 15 ~~times~~ for a 35-year~~s~~ inversion. The ~~PPVI~~PP method makes multi-decadal global inversions of long-lived atmospheric trace gases more feasible. It~~It~~ will be implemented in the CAMS reanalysis setup which provides regular updates of multidecadal emission estimates by assimilating surface and satellite observations.

Data Availability. NOAA ESRL methane observations used in this study are available on Zenodo in the input folder of the TM5-4DVAR-PP code (https://doi.org/10.5281/zenodo.6326373, Pandey et al., 2022).

~~NOAA GMD ESRL methane mole fraction observations are available at https://www.esrl.noaa.gov/gmd/dv/data/. last access: 27-03-2021.~~

Code availability. The TM5-4DVAR-PP version 1.0-beta-1 code used in this study for the simulations can be downloaded from Zenodo (https://doi.org/10.5281/zenodo.6326373, Pandey et al., 2022). The TM5 model is described in detail on~~on~~ http://tm5.sourceforge.net/. ~~and the source codes of the TM5-4DVAR inversion system are available at https://sourceforge.net/projects/tm5/.~~

Author contributions. The study was designed by SH and AJ~~FC~~. SP and AJ developed the ~~PPVI~~PP. SP implemented the ~~PPVI~~PP method on TM5-4DVAR and did the performance test simulations. SP wrote the manuscript using contributions from all the co-authors.

Acknowledgements. We thank the efforts of NOAA and other surface observations networks for producing and maintaining the vital long record of global methane ~~surface~~ observations. The computations for this study were carried out on the Dutch national supercomputer Cartesius (https://userinfo.surfsara.nl/systems/cartesius; last access: 27-03-2020) maintained by SURFSara. SP and AJ were funded for this study by the Copernicus Atmosphere Monitoring Service, implemented by the European Centre for Medium-Range Weather Forecasts on behalf of the European Commission (grant no. CAMS73).

Competing interests. The authors declare that they have no competing interests.

References

Basu, S., Guerlet, S., Butz, A., Houweling, S., Hasekamp, O., Aben, I., Krummel, P., Steele, P., Langenfelds, R., Torn, M., Biraud, S., Stephens, B., Andrews, A., and Worthy, D.: Global CO2 fluxes estimated from GOSAT retrievals of total column CO2, Atmos. Chem. Phys., 13, 8695–8717, doi:10.5194/acp-13-8695- 2013, 2013.

Bergamaschi, P., Krol, M., Meirink, J. F., Dentener, F., Segers, A., van Aardenne, J., Monni, S., Vermeulen, A. T., Schmidt, M., Ramonet, M., Yver, C., Meinhardt, F., Nisbet, E. G., Fisher, R. E., O'Doherty, S., and Dlugokencky, E. J.: Inverse modeling of European CH4 emissions 2001–2006, J. Geophys. Res., 115, D22309, doi:10.1029/2010JD014180, 2010.

Chevallier, F., Fisher, M., Peylin, P., Serrar, S., Bousquet, P., Bréon, F. M., Chédin, A. and Ciais, P.: Inferring CO2 sources and sinks from satellite observations: Method and application to TOVS data, J. Geophys. Res. Atmos., 110(24), 1–13, doi:10.1029/2005JD006390, 2005.

Chevallier, F., Breon, F.-M., and Rayner, P. J.: Contribution of the Orbiting Carbon Observatory to the estimation of CO2 sources and sinks: Theoretical study in a variational data assimilation framework, J. Geophys. Res.-Atmos., 112, d09307, https://doi.org/10.1029/2006JD007375, 2007.

Chevallier, F.: On the parallelization of atmospheric inversions of CO_2 surface fluxes within a variational framework, Geosci. Model Dev., 6, 783–790, https://doi.org/10.5194/gmd-6-783-2013, 2013.

Dee, D. P., Uppala, S. M., Simmons, A. J., Berrisford, P., Poli, P., Kobayashi, S., Andrae, U., Balmaseda, M. A., Balsamo, G., Bauer, P., Bechtold, P., Beljaars, A. C. M., van de Berg, L., Bidlot, J., Bormann, N., Delsol, C., Dragani, R., Fuentes, M., Geer, A. J., Haimberger, L., Healy, S. B., Hersbach, H., Hólm, E. V., Isaksen, L., Kållberg, P., Köhler, M., Matricardi, M., McNally, A. P., Monge-Sanz, B. M., Morcrette, J.-J., Park, B.-K., Peubey, C., de Rosnay, P., Tavolato, C., Thépaut, J.-N., and Vitart, F.: The ERA-Interim reanalysis: Configuration and performance of the data assimilation system, Q. J. Roy. Meteor. Soc., 137, 553–597, 2011.

Dlugokencky, E. J., Nisbet, E. G., Fisher, R. and Lowry, D.: Global atmospheric methane: Budget, changes and dangers, Philos. Trans. R. Soc. A Math. Phys. Eng. Sci., 369(1943), 2058–2072, doi:10.1098/rsta.2010.0341, 2011.

Dlugokencky, E. J., Crotwell, A. M., Mund, J. W., Crotwell, M. J., and Thoning, K. W.: Atmospheric Methane Dry Air Mole Fractions from the NOAA GML Carbon Cycle Cooperative Global Air Sampling Network, Version: 2020-07, https://doi.org/10.15138/VNCZ-M766, 2020.

Fisher, M. and Courtier, P.: Estimating the covariance matrices of analysis and forecast error in variational data assimilation, in: ECMWF Technical Memorandum 220, ECMWF, Reading, UK, doi:10.21957/1dxrasjit, 1995

~~Ganesan, A. L., Schwietzke, S., Poulter, B., Arnold, T., Lan, X., Rigby, M., Vogel, F. R., van der Werf, G. R., Janssens-Maenhout, G., Boesch, H., Pandey, S., Manning, A. J., Jackson, R. B., Nisbet, E. G. and Manning, M. R.: Advancing Scientific Understanding of the Global Methane Budget in Support of the Paris Agreement, Global Biogeochem. Cycles, 33(12), 1475–1512, doi:10.1029/2018GB006065, 2019.~~

Gurney, K., Law, R., Denning, A., Rayner, P., Baker, D., Bousquet, P., Bruhwiler, L., Chen, H., Ciais, P., Fan, S., Fung, I., Gloor, M., Heimann, M., Higuchi, K., John, J., Maki, T., Maksyu- tov, S., Ken, M., Peylin, P., Prather, M., Pak, B. C., Randerson, J., Sarmiento, J., Taguchi, S., Takahashi, T., and Yuen, C.-W.: Towards robust regional estimates of CO2 sources and sinks using atmospheric transport models, Nature, 415, 626–630, doi:10.1038/415626a, 2002.

Houweling, S., Krol, M., Bergamaschi, P., Frankenberg, C., Dlugokencky, E. J., Morino, I., Notholt, J., Sherlock, V., Wunch, D., Beck, V., Gerbig, C., Chen, H., Kort, E. A., Röckmann, T. and Aben, I.: A multi-year methane inversion using SCIAMACHY, accounting for systematic errors using TCCON measurements, Atmos. Chem. Phys., 14(8), 3991–4012, doi:10.5194/acp-14-3991-2014, 2014.

Krol, M., Houweling, S., Bregman, B., van den Broek, M., Segers, A., van Velthoven, P., Peters, W., Dentener, F., and Bergamaschi, P.: The two-way nested global chemistry-transport zoom model TM5: algorithm and applications, Atmos. Chem. Phys., 5, 417– 432, doi:10.5194/acp-5-417-2005, 2005.

Maasakkers, J. D., Jacob, D. J., Sulprizio, M. P., Scarpelli, T. R., Nesser, H., Sheng, J. X., Zhang, Y., Hersher, M., Anthony Bloom, A., Bowman, K. W., Worden, J. R., Janssens-Maenhout, G. and Parker, R. J.: Global distribution of methane emissions, emission trends, and OH concentrations and trends inferred from an inversion of GOSAT satellite data for 2010-2015, Atmos. Chem. Phys., 19(11), 7859–7881, doi:10.5194/acp-19-7859-2019, 2019.

Myhre, G., Shindell, D., Bréon, F.-M., Collins, W., Fuglestvedt, J., Huang, J., Koch, D., Lamarque, J.-F., Lee, D., Mendoza, B., Nakajima, T., Robock, A., Stephens, G., Takemura, T., and Zhang, H.: Anthropogenic and Natural Radiative Forcing, in:

Climate Change 2013: The Physical Science Basis. Contribution ofWorking Group I to the Fifth Assessment Report of the Intergovernmental Panel on Climate Change, Cambridge University Press, Cambridge, UK and New York, NY, USA, 2013.

Meirink, J. F., Bergamaschi, P., and Krol, M. C.: Four- dimensional variational data assimilation for inverse modelling of atmospheric methane emissions: method and comparison with synthesis inversion, Atmos. Chem. Phys., 8, 6341–6353, doi:10.5194/acp-8-6341-2008, 2008.

Naus, S., Montzka, S. A., Pandey, S., Basu, S., Dlugokencky, E. J. and Krol, M.: Constraints and biases in a tropospheric two-box model of OH, Atmos. Chem. Phys., 407–424, 2019.

Naus, S., Montzka, S. A., Patra, P. K. and Krol, M. C.: A three-dimensional-model inversion of methyl chloroform to constrain the atmospheric oxidative capacity, Atmos. Chem. Phys., 21(6), 4809–4824, doi:10.5194/acp-21-4809-2021, 2021.

~~Nisbet, E. G., Manning, M. R., Dlugokencky, E. J., Fisher, R. E., Lowry, D., Michel, S. E., … and White, J. W. C.: Very Strong Atmospheric Methane Growth in the 4 Years 2014–2017: Implications for the Paris Agreement, Global Biogeochem. Cycles, 33(3), 318–342, doi:10.1029/2018GB006009, 2019.~~

~~Pandey, S., Houweling, S., Krol, M., Aben, I., Monteil, G., Nechita-Banda, N., Dlugokencky, E. J., Detmers, R., Hasekamp, O., Xu, X., Riley, W. J., Poulter, B., Zhang, Z., McDonald, K. C., White, J. W. C., Bousquet, P. and Röckmann, T.: Enhanced methane emissions from tropical wetlands during the 2011 la Niña, Sci. Rep., 7 (October 2016), 1–8, doi:10.1038/srep45759, 2017.~~

Pandey, S., Houweling, S., Krol, M., Aben, I., Chevallier, F., Dlugokencky, E. J., Gatti, L. V., Gloor, E., Miller, J. B., Detmers, R., Machida, T. and Röckmann, T.: Inverse modeling of GOSAT-retrieved ratios of total column CH4 and CO2 for 2009 and 2010, Atmos. Chem. Phys., 16(8), 5043–5062, doi:10.5194/acp-16-5043-2016, 2016.

Pandey, S., Houweling, S., Krol, M. and Aben, I.: Influence of Atmospheric Transport on Estimates of Variability in the Global Methane Burden Geophysical Research Letters, Geophys. Res. Lett., doi:10.1029/2018GL081092, 2019.

Pandey, Sudhanshu, Houweling, Sander, and Segers, Arjo. TM5-4DVAR-PP Version 1.0-beta.1. Zenodo. https://doi.org/10.5281/zenodo.6326373, 2022

Peters, W., Miller, J. B., Whitaker, J., Denning, A. S., Hirsch, A., Krol, M. C., Zupanski, D., Bruhwiler, L., and Tans, P. P.: An ensemble data assimilation system to estimate CO2 surface fluxes from atmospheric trace gas observations, J. Geophys. Res., 110, D24304, doi:10.1029/2005JD006157, 2005.

~~Rigby, M., Montzka, S. A., Prinn, R. G., White, J. W. C., Young, D., O'Doherty, S., Lunt, M. F., Ganesan, A. L., Manning, A. J., Simmonds, P. G., Salameh, P. K., Harth, C. M., Mühle, J., Weiss, R. F., Fraser, P. J., Steele, L. P., Krummel, P. B., McCulloch, A. and Park, S.: Role of atmospheric oxidation in recent methane growth, Proc. Natl. Acad. Sci., 114(21), 5373–5377, doi:10.1073/pnas.1616426114, 2017.~~

Saunois, M., R. Stavert, A., Poulter, B., Bousquet, P., G. Canadell, J., B. Jackson, … and Zhuang, Q.: The global methane budget 2000-2017, Earth Syst. Sci. Data, 12(3), 1561–1623, doi:10.5194/essd-12-1561-2020, 2020.

Segers, A. and Houweling, S.: Validation of the CH4 surface flux inversion - reanalysis 1990-2017, 1–40, 2020. Available at https://atmosphere.copernicus.eu/sites/default/files/2021-02/CAMS73_2018SC2_D73.2.4.1-2020_202012_validation_CH4_1990-2019_v2.pdf Last access: 27-3-2021

~~Schaefer, H., Fletcher, S. E. M., Veidt, C., Lassey, K. R., Brailsford, G. W., Bromley, T. M., Dlugokencky, E. J., Michel, S. E., Miller, J. B., Levin, I., Lowe, D. C., Martin, R. J., Vaughn, B. H., and White, J. W. C.: A 21st century shift from fossil-fuel to biogenic methane emissions indicated by 13CH4, Science, 10.1126/science.aad2705, 2016.~~

~~Worden, J. R., Bloom, A. A., Pandey, S., Jiang, Z., Worden, H. M., Walker, T. W., Houweling, S. and Röckmann, T.: Reduced biomass burning emissions reconcile conflicting estimates of the post-2006 atmospheric methane budget, Nat. Commun., 8(1), 2227, doi:10.1038/s41467-017-02246-0, 2017.~~

Williams, J. E., Boersma, K. F., Le Sager, P., and Verstraeten, W. W.: The high-resolution version of TM5-MP for optimized satellite retrievals: description and validation, Geosci. Model Dev., 10, 721–750, https://doi.org/10.5194/gmd-10-721-2017, 2017.

Zhang, Y., Jacob, D. J., Maasakkers, J. D., Sulprizio, M. P., Sheng, J.-X., Gautam, R., and Worden, J.: Monitoring global tropospheric OH concentrations using satellite observations of atmospheric methane, Atmos. Chem. Phys., 18, 15959–15973, https://doi.org/10.5194/acp-18-15959-2018, 2018.

Zhang, Y., J. Jacob, D., Lu, X., D. Maasakkers, J., R. Scarpelli, T., Sheng, J. X., Shen, L., Qu, Z., P. Sulprizio, M., Chang, J., Anthony Bloom, A., Ma, S., Worden, J., J. Parker, R. and Boesch, H.: Attribution of the accelerating increase in atmospheric

methane during 2010-2018 by inverse analysis of GOSAT observations, Atmos. Chem. Phys., 21(5), 3643–3666, doi:10.5194/acp-21-3643-2021, 2021.

Table 1~~:~~ Wall ~~clock~~ time comparison for the inversions performed in this study. Wall ~~clock~~ time projections for a hypothetical 35~~-~~ year~~s~~ inversion are also given.

Model runs		**Serial**	~~**PPVI**~~**PP**
One year forward or adjoint run		15 minutes	
1999-2010 inversion	1 iteration (forward + adjoint TM5 run)	5 hours	55 minutes
	Inversion with 19 iterations	101 hours	20 hours
1985-2020 inversion*	1 iteration (forward + adjoint TM5 run)	16 hours	55 minutes
	Inversion with 50 iterations	34 days	56 hours

*Projection based on the 1999-2010 inversion

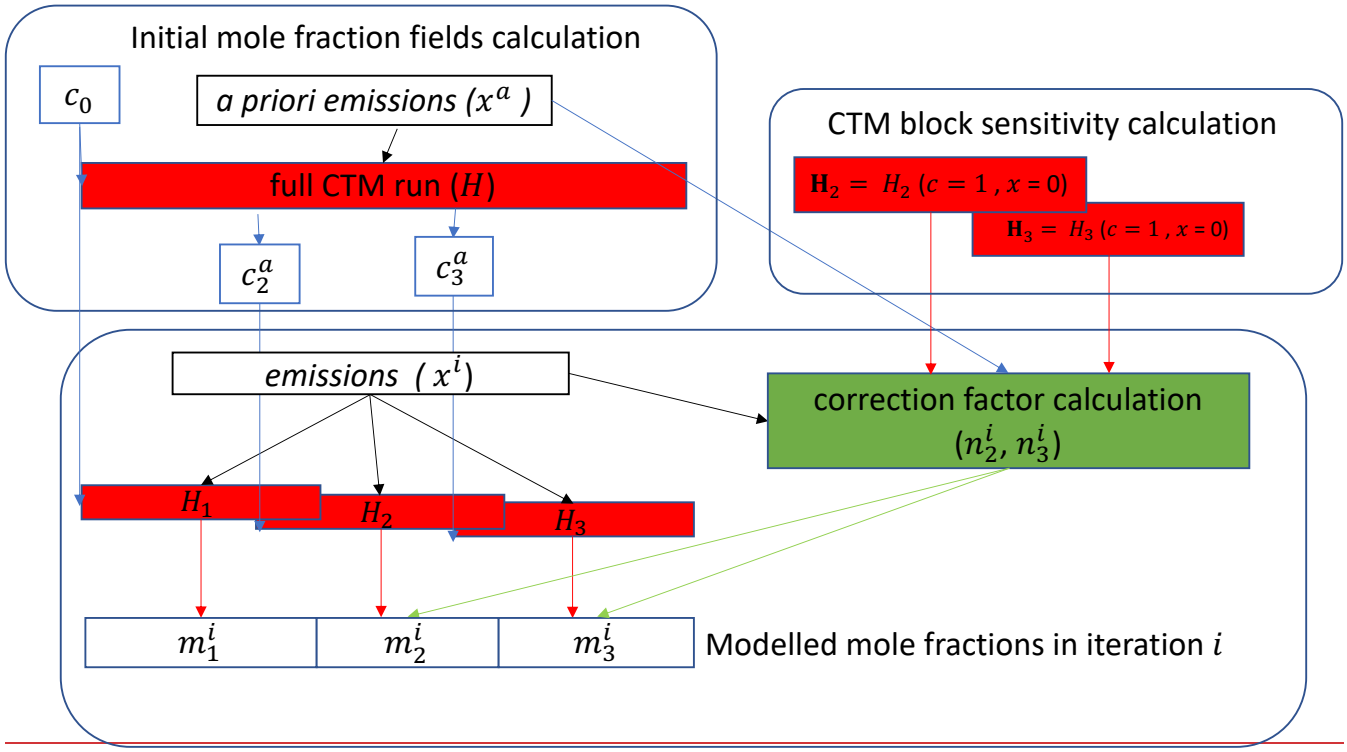
Initial mole fraction fields calculation
c_0
a priori emissions (x^a)
full CTM run (H)
c_2^a
c_3^a
CTM block sensitivity calculation
$\mathbf{H}_2 = H_2\,(c = 1\,, x = 0)$
$\mathbf{H}_3 = H_3\,(c = 1\,, x = 0)$
emissions (x^i)
correction factor calculation
(n_2^i, n_3^i)
H_1
H_2
H_3
m_1^i
m_2^i
m_3^i
Modelled mole fractions in iteration i

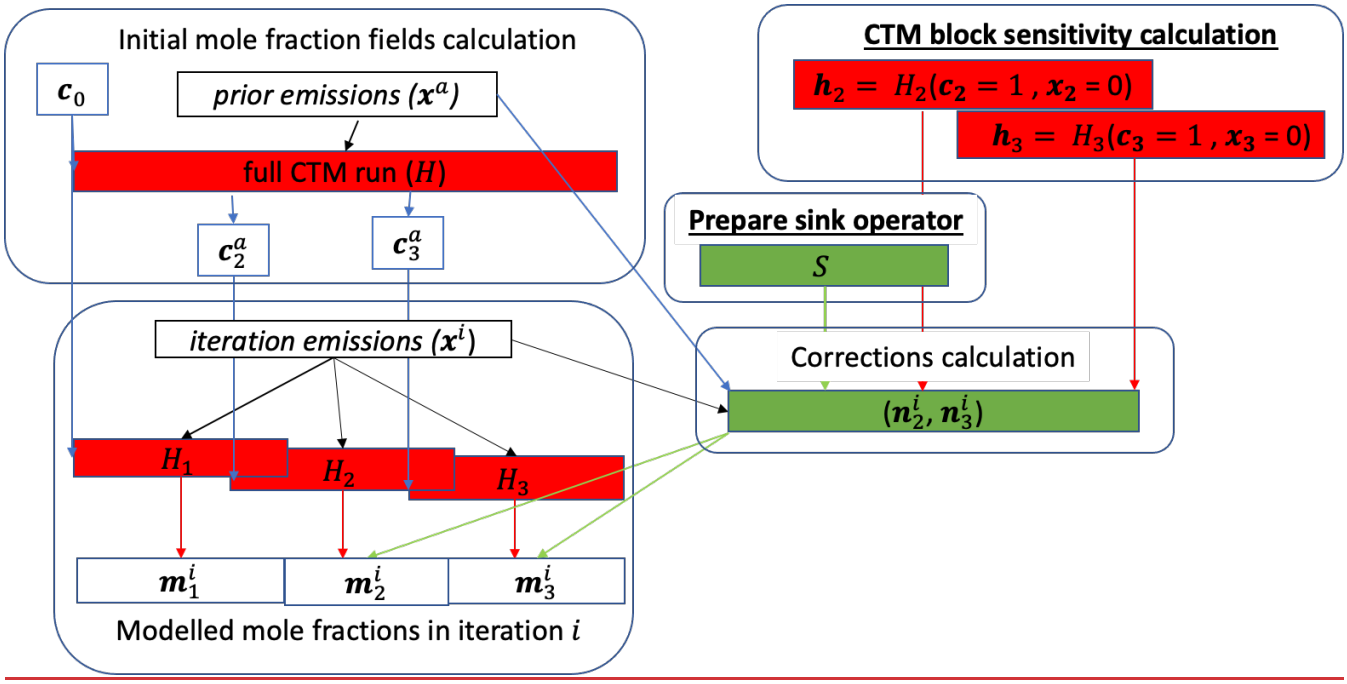
Initial mole fraction fields calculation
$\boldsymbol{c}_0$
prior emissions ($\boldsymbol{x}^a$)
full CTM run (H)
$\boldsymbol{c}_2^a$
$\boldsymbol{c}_3^a$
CTM block sensitivity calculation
$\boldsymbol{h}_2 = H_2(\boldsymbol{c}_2 = 1\,, \boldsymbol{x}_2 = 0)$
$\boldsymbol{h}_3 = H_3(\boldsymbol{c}_3 = 1\,, \boldsymbol{x}_3 = 0)$
Prepare sink operator
S
iteration emissions ($\boldsymbol{x}^i$)
Corrections calculation
$(\boldsymbol{n}_2^i, \boldsymbol{n}_3^i)$
H_1
H_2
H_3
$\boldsymbol{m}_1^i$
$\boldsymbol{m}_2^i$
$\boldsymbol{m}_3^i$
Modelled mole fractions in iteration i

Figure ~~1~~1~~:~~ Schematic diagram of ~~a~~the PP~~VI~~ methane inversion's ~~method in~~ forward mode, which computes ~~used to calculate modelled~~ mole fractions $\boldsymbol{m^i}$ in~~of~~ iteration i. The subscripts ~~represent~~ denote the ~~time~~ block numbers (except for $\boldsymbol{c_0}$, which is the initial mole fraction field at the start of the inversion**).** For ~~the~~ block 1, the initial mole fraction field ~~$\boldsymbol{c_1^a = c_0}$~~ $\boldsymbol{(c_1^a = c_0)}$ and mole fraction ~~no~~ correction ~~factor~~ vector ($\boldsymbol{n^i}$) is not needed~~used~~. The overlap between the successive blocks ($\boldsymbol{H_1}$, $\boldsymbol{H_2}$, $\boldsymbol{H_3}$) ~~represent~~ represent the ~~block overlap~~overlap period ~~period~~, where the modelled mole fractions from the preceding block are used in the inversion~~ed in $\boldsymbol{m^i}$~~. The "CTM block sensitivity calculation" and "Prepare sink ~~–~~operator" steps of the PP method are implemented in this study, whereas the rest are from Chevallier (2013).

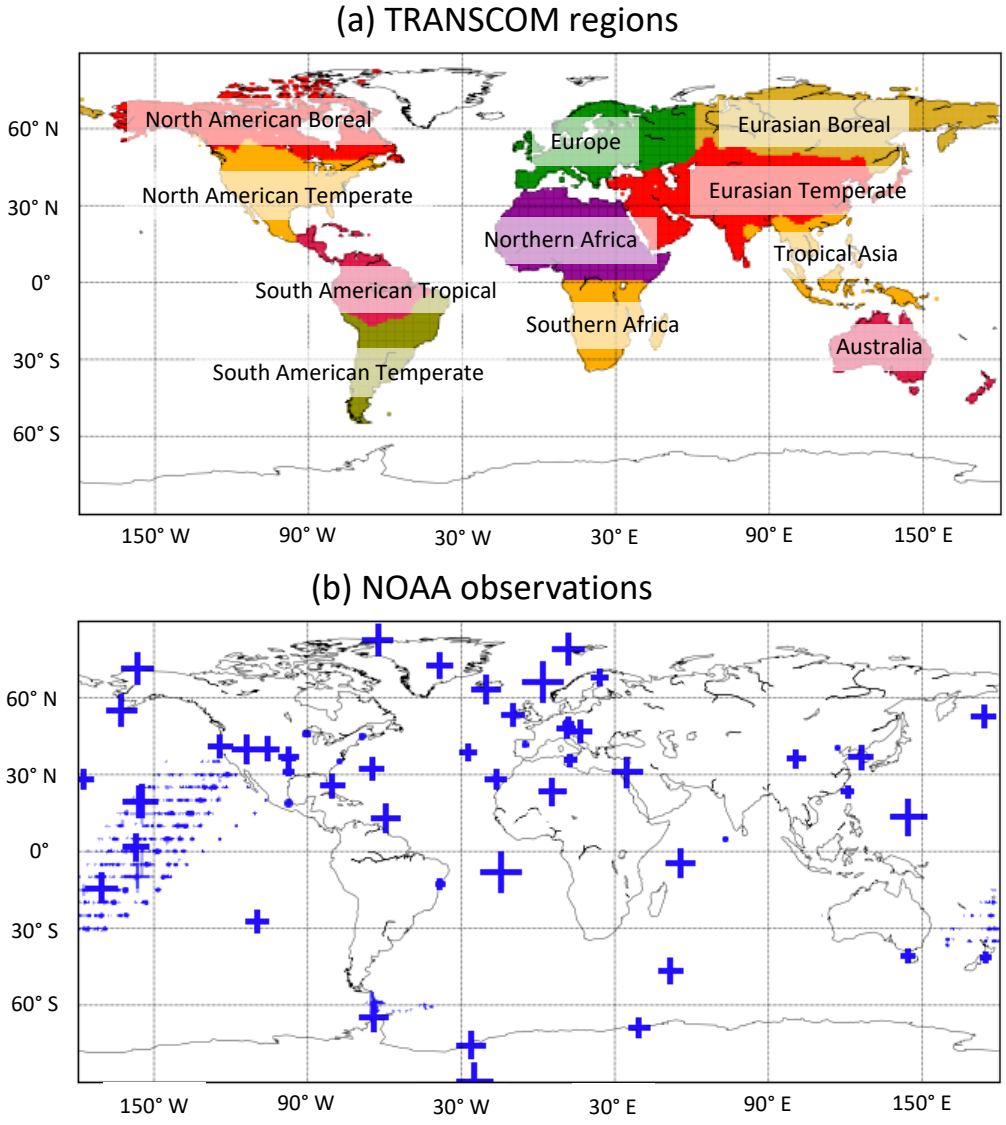

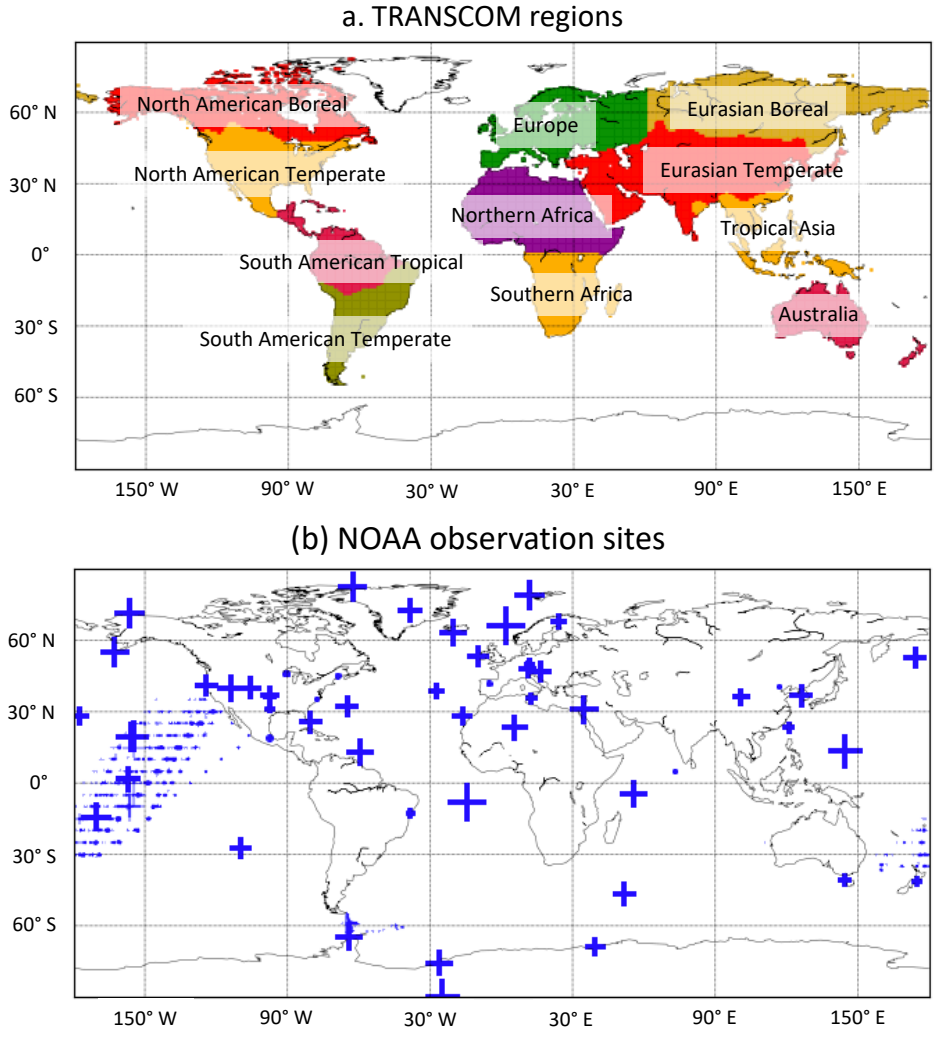

Figure 2: (a) Definition of the TRANSCOM regions (Gurney et al., 2002). (b) Locations of NOAA methane observation sites used in this study. The size of the symbol "+" is proportional to the number of observations assimilated from each site.

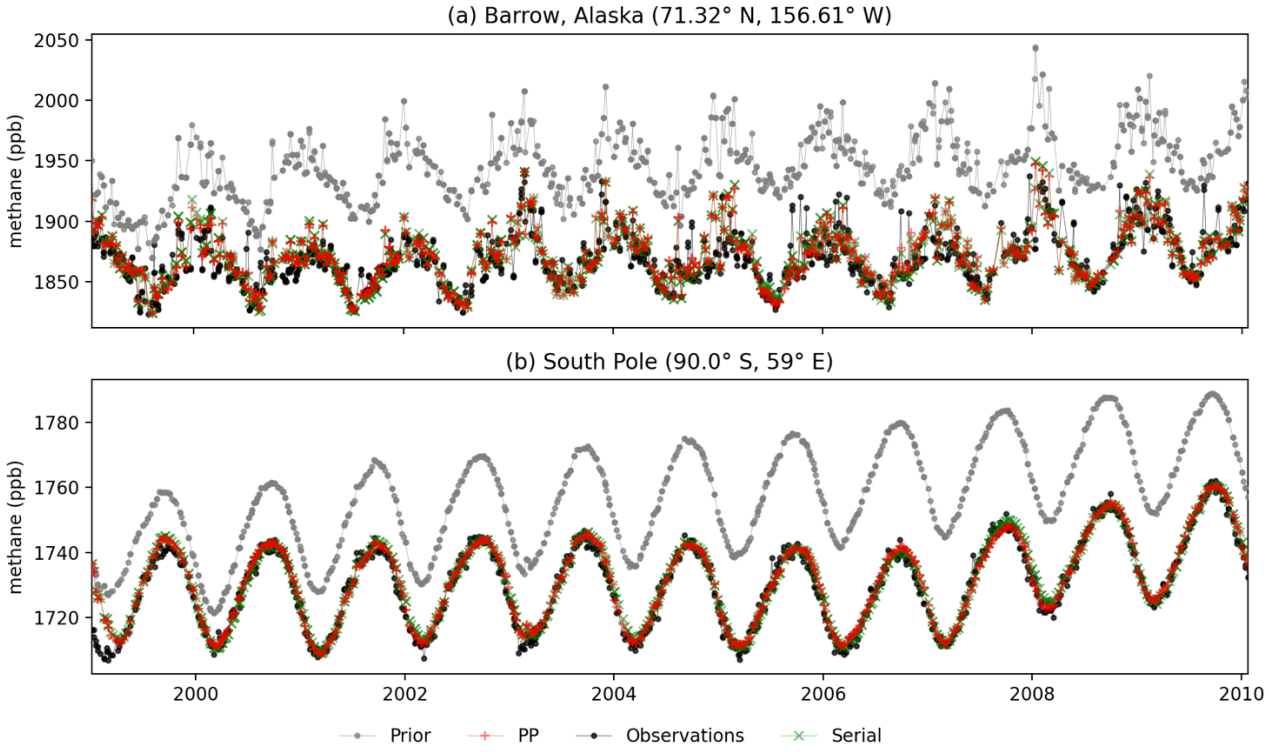
(a) Barrow, Alaska (71.32° N, 156.61° W)
methane (ppb)
2050
2000
1950
1900
1850
(b) South Pole (90.0° S, 59° E)
methane (ppb)
1780
1760
1740
1720
2000
2002
2004
2006
2008
2010
Prior
PP
Observations
Serial

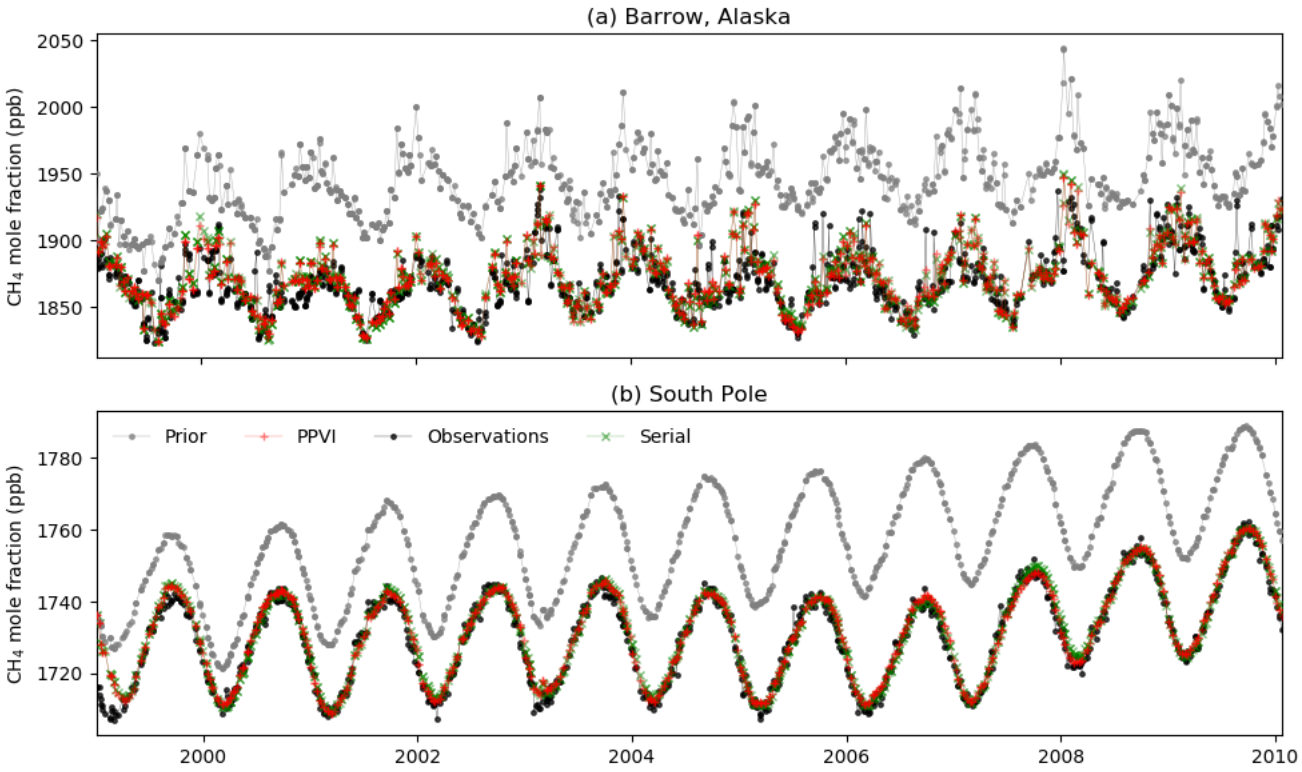

Figure 3~~:~~ Modelled and observed methane mole fractions at the two remote background NOAA stations~~.~~, Barrow, Alaska ~~in the Northern~~ is shown in panel (a), and the South Pole is shown in panel ~~Southern~~ (b) ~~hemisphere~~.

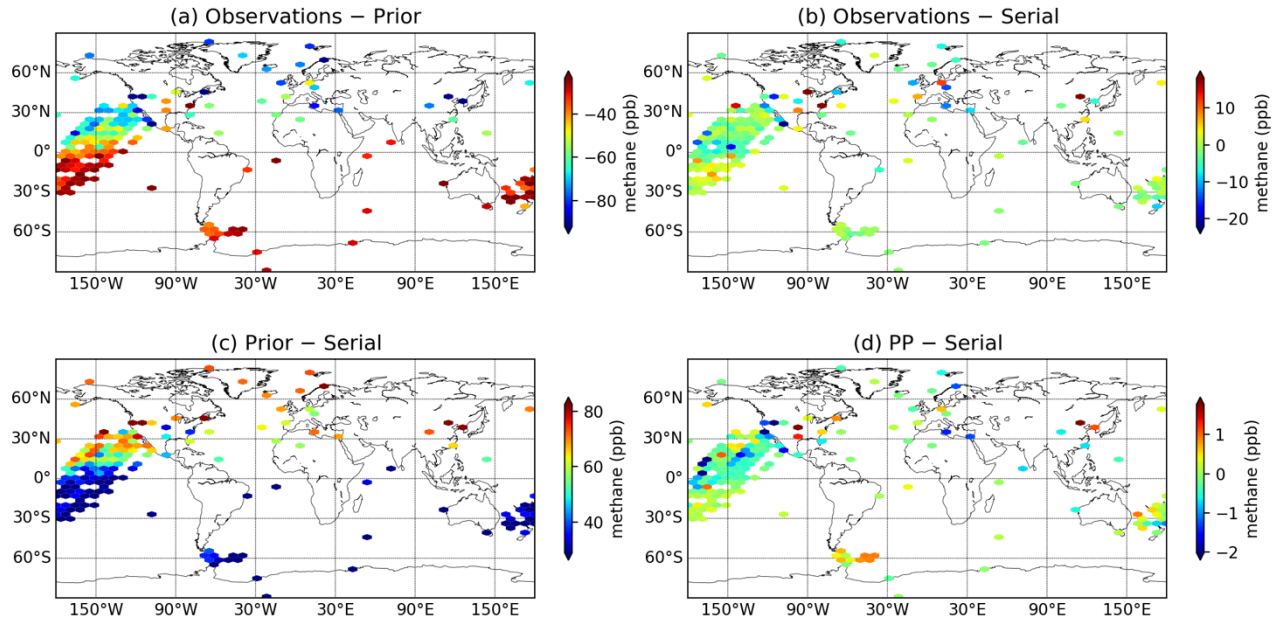

Figure 4 Methane mole fraction differences at the observation sites (see Figure 2.b). Panel (a), (b), (c) and (d) show the average difference between observations and prior, observation and serial, prior and serial, and PP and serial, respectively. The color scale range is set at mean ± 1 standard deviation of the plotted values.

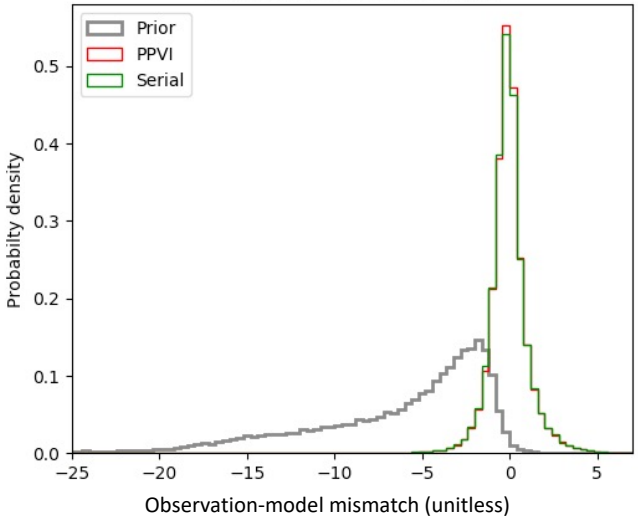

~~**Figure 4: Probability density functions of the observation-model mismatches weighted with their uncertainties used in the inversions.**~~

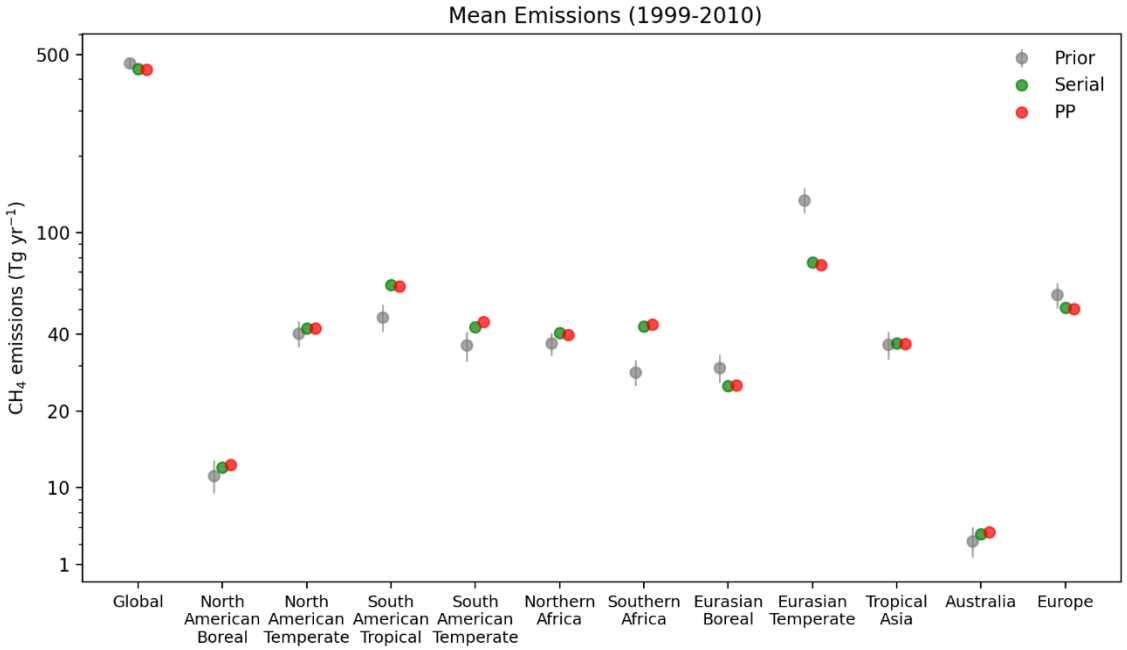

685

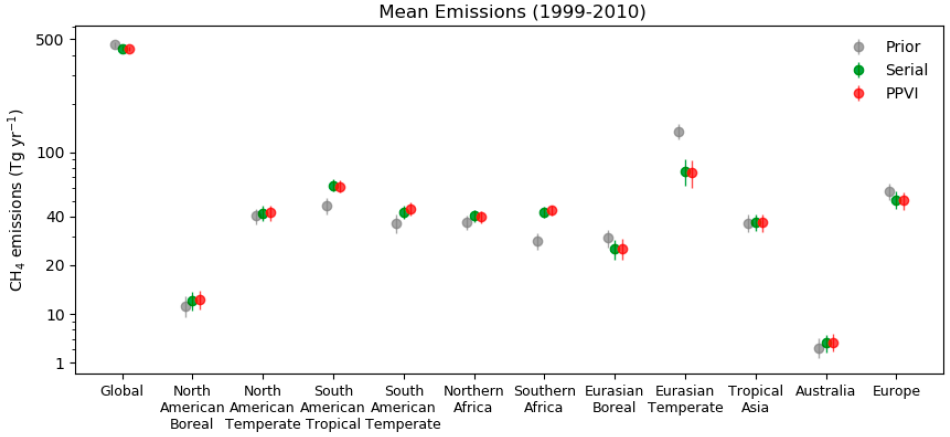

Figure ~~55:~~ Total methane ~~Mean~~ emission estimates of ~~estimates of~~ the inversions for the globe and TRANSCOM regions ~~(see Figure 1)~~, averaged over 1999-2010 (see Figure 1). The vertical lines~~bars~~ on the markers show the ±2σ uncertainties of the prior emissions.

690

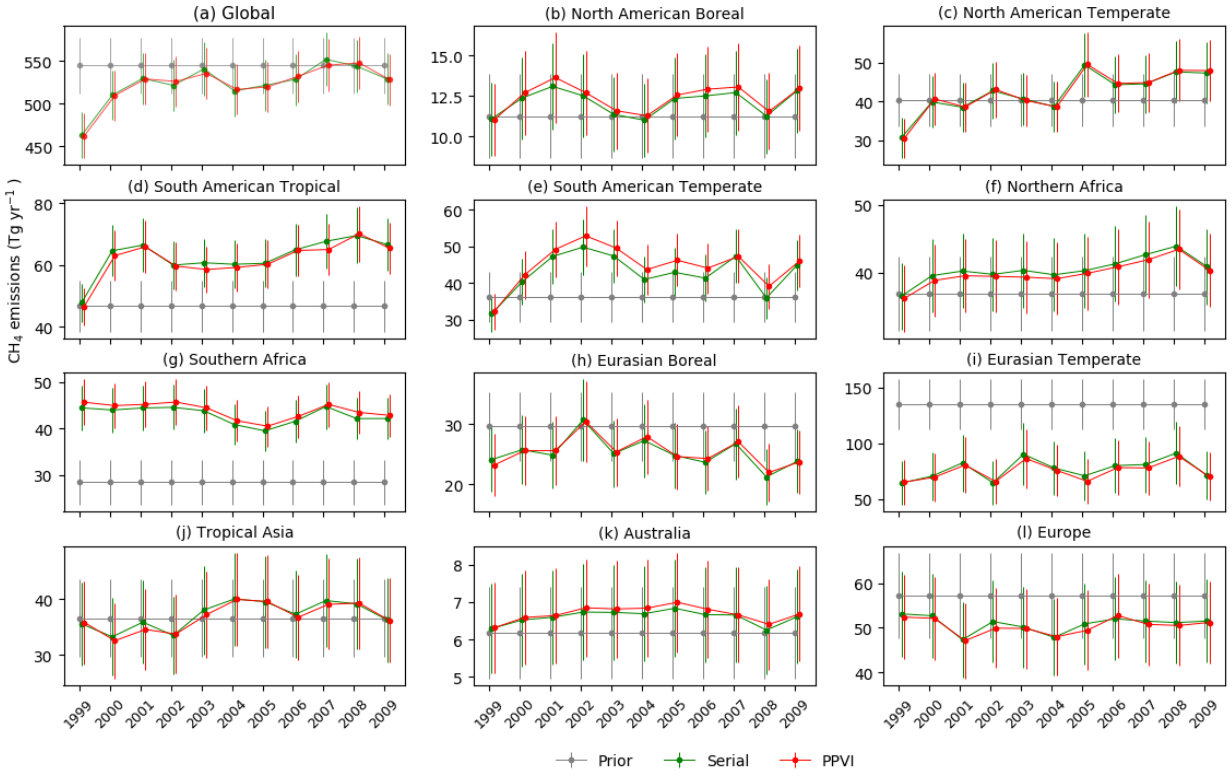
(a) Global
(b) North American Boreal
(c) North American Temperate
(d) South American Tropical
(e) South American Temperate
(f) Northern Africa
(g) Southern Africa
(h) Eurasian Boreal
(i) Eurasian Temperate
(j) Tropical Asia
(k) Australia
(l) Europe
CH4 emissions (Tg yr−1)
1999
2000
2001
2002
2003
2004
2005
2006
2007
2008
2009
Prior
Serial
PPVI

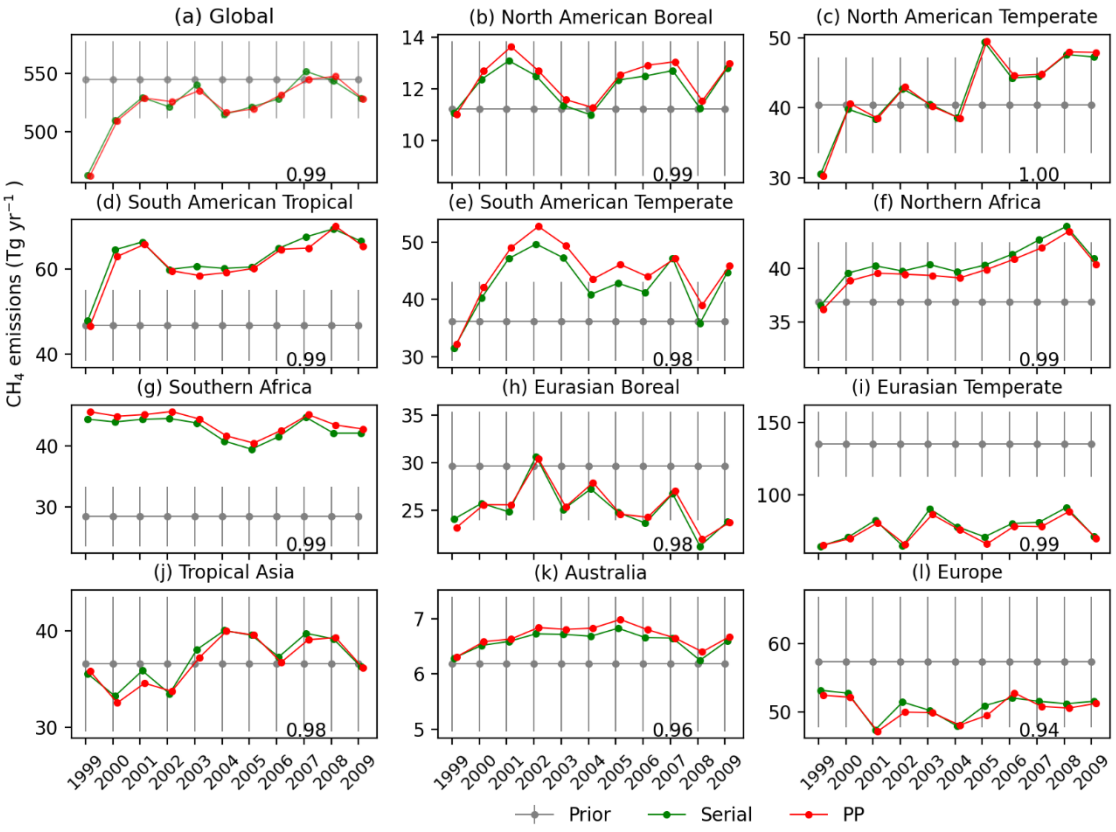

695

Figure ~~66:~~ Annual methane e~~E~~mission estimates of the ~~PPVI~~PP and serial inversions for the globe and the TRANSCOM regions. The vertical bars show the ±2σ- uncertainties of the prior emissions. The correlation coefficients of PP and serial time series are given at the bottom of each panel.

700

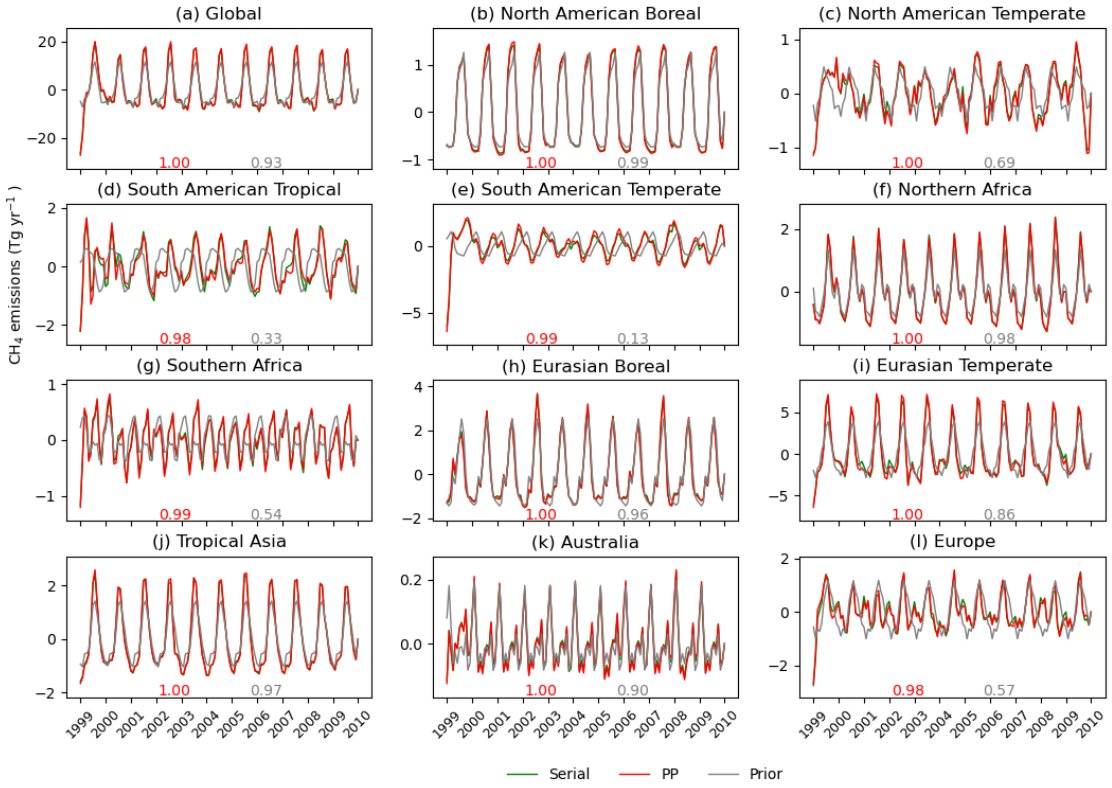

Figure 7 Intra-annual variation of the PP and serial emissions for the TRANSCOM regions. The correlation coefficients of the PP (red) and prior (grey) time series with the serial time series are given at the bottom of each panel.